THE JOURNAL OF PHYSICAL CHEMISTRY C

Article

pubs.acs.org/JPCC

Probing Structural, Electronic, and Magnetic Properties of Iron-Doped Semiconductor Clusters $Fe_2Ge_n^{-/0}$ (n = 3−12) via Joint Photoelectron Spectroscopy and Density Functional Study

Xiao-Qing Liang,[†,∥] Xiao-Jiao Deng,[‡] Sheng-Jie Lu,[‡] Xiao-Ming Huang,[§] Ji-Jun Zhao,*[,†] Hong-Guang Xu,*[,‡] Wei-Jun Zheng,[‡] and Xiao Cheng Zeng*[,∥,⊥]

[†]Key Laboratory of Materials Modification by Laser, Ion and Electron Beams, Dalian University of Technology, Ministry of Education, Dalian 116024, China

[‡]Beijing National Laboratory for Molecular Science, State Key Laboratory of Molecular Reaction Dynamics, Institute of Chemistry, Chinese Academy of Sciences, Beijing 100190, China

[§]School of Ocean Science and Technology, Dalian University of Technology, Panjin Campus, Panjin 124221, China

[∥]Department of Chemistry, University of Nebraska, Lincoln, Nebraska 68588, United States

[⊥]Collaborative Innovation Center of Chemistry for Energy Materials, University of Science and Technology of China, Hefei 230026, China

Supporting Information

ABSTRACT: We present a joint experimental and theoretical study on double iron atom doped germanium clusters, $Fe_2Ge_n^{-/0}$ (n = 3−12). The experimental photoelectron spectra of cluster anions are reasonably reproduced by theoretical simulations. The low-lying structures of the iron-doped semiconductor clusters are obtained by using an ab initio computation-based genetic-algorithm global optimization method. We find that the smaller-sized $Fe_2Ge_n^-$ (n = 3−8) clusters adopt bipyramid-based geometries, while the larger ones ($n \geq 9$) adopt polyhedral cagelike structures with one interior Fe atom. Interestingly, starting from n = 8, the most stable anionic clusters $Fe_2Ge_n^-$ exhibit structures that are different from that of their neutral counterparts Fe_2Ge_n. Robust ferromagnetic interaction is found between the two doped iron atoms in the neutral clusters Fe_2Ge_n, while the total spin moment always remains at 4 μ_B for all the neutral double iron atom doped germanium clusters up to n = 12. This behavior is in stark contrast to the magnetic quenching behavior typically observed in germanium clusters doped with a single Fe atom.

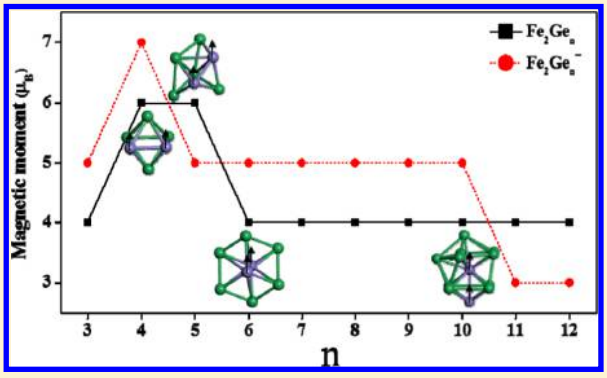

1. INTRODUCTION

Doping, the intentional incorporation of impurities into materials, is a widely used strategy to modify or tune physical properties of semiconductor materials. Doping selected iron-group atoms into a semiconductor solid may induce local ferromagnetism and yield a so-called dilute magnetic semiconductor[1] for potential spintronic applications. Analogous to doping bulk materials, doping iron-group atoms into semiconductor clusters can also introduce local spin moment and convert a nonmagnetic nanocluster into a magnetic one.[2,3]

Among various semiconductor clusters, germanium clusters have attracted increasing attention due in part to the expectation that germanium is a potential alternative to silicon in some special sectors of the microelectronic industry.[4,5] Over the past 10 years, many experimental and theoretical studies of unary transitional metal (TM)-doped germanium nanoclusters, $TMGe_n$, have been reported.[6−16] The major focus of most previous experimental studies was placed on producing and stabilizing Ge cagelike structures. For example, Wang et al.[6] synthesized an intermetalloid cluster $CoGe_{10}^{3-}$ with the Archimedean pentagonal prismatic structure. Zhou et al.[7] performed experimental measurements and reported another pentagonal prismatic Zintl ion, $FeGe_{10}^{3-}$, whose cage structure can encompass an interstitial iron atom. Among other experimental techniques, photoelectron spectroscopy and mass spectroscopy are two common tools employed to study $TMGe_n^-$ clusters.[8−10] TM dopants in the latter include 3d-TM (Cr−Mn, Cu, and Zn), 4d-TM (Y−Nb), and 5d-TM (Lu−Ta). Recently, $RuGe_n^-$ (n = 3−12), $AuGe_n^-$ (n = 2−12), $TiGe_n^-$ (n = 2−12), VGe_n^- (n = 3−12), and $CoGe_n^-$ (n = 3−11) clusters have also been experimentally studied by the Zheng group.[11−16]

Received: January 30, 2017
Revised: February 28, 2017
Published: March 3, 2017

ACS Publications © 2017 American Chemical Society

DOI: 10.1021/acs.jpcc.7b00943
J. Phys. Chem. C 2017, 121, 7037−7046

On the theoretical side, the structural evolution and electronic properties of $TMGe_n$ clusters, such as WGe_n (n = 1−17),[17] have been intensively studied, and the critical size of W-encapsulated Ge_n structures and the fullerene-like $W@Ge_n$ clusters emerge at n = 12 and n = 14, respectively. For $NiGe_n$ (n = 1−20), $CuGe_n$ (n = 2−13), $XGe_{10}^{0/-}$ (X═Cu, Au), and $MnGe_n$ (n = 2−15) clusters, the critical size to form TM-encapsulated Ge_n clusters is n = 10.[18−21] On the basis of the anion photoelectron spectroscopy in combination with density functional theory (DFT) calculations, VGe_n (n = 3−12),[14] $CoGe_n$ (n = 2−11),[22] and $RuGe_n$ (n = 3−12)[11] clusters have been studied, from which the structural evolution from exohedral to endohedral geometries was suggested. Theoretical studies also predicted that TM-doped germanium clusters tend to possess higher magnetic moments than the silicon counterparts. For example, $CrGe_n$ clusters[23] up to n = 13 are magnetic with high spin multiplicity (quintet or septet), whereas $CrSi_n$ are nonmagnetic clusters.[24] $MnGe_n$ and $CoGe_n$ (n = 1−13) clusters[22] entail 1 or 3 μ_B magnetic moments, contrary to the magnetic quenching in $MnSi_n$ (n = 1−15)[25] at n = 8 and $CoSi_n$ (n = 2−14)[26] at n = 7. Tang et al.[27] studied the geometric, optical, and magnetic properties of the endohedral $Ge_{12}M$ (M = Sc−Ni) clusters using the relativistic all-electron DFT method. They found that the magnetic moments of $Ge_{12}M$ vary from 1 to 5 μ_B. Single Fe atom doped germanium clusters, $FeGe_n$ (n = 1−8) and $FeGe_n$ (n = 9−16), have been independently studied using DFT calculations by two research groups.[28,29] Magnetic moments of most clusters are stable at 2 μ_B, except for n = 9, 13, 14, and 15 whose magnetic moments are quenched.

Most theoretical efforts thus far have been devoted to understanding single TM atom doped semiconductor clusters, while much less effort has been devoted to the effects of multiple TM atoms on the magnetism of doped semiconductor clusters.[30−35] For Fe, a single atom carries a magnetic moment of 4 μ_B, whereas the bulk solid possesses a magnetic moment of 2.2 μ_B/atom below the Curie temperature.[36,37] With multiple Fe atoms as dopant, higher magnetic moments are expected in clusters than in the bulk. Single Fe atom doped germanium clusters $FeGe_n$ (n = 1−16) are shown to exhibit magnetic moments of either zero or 2 μ_B. Would two Fe atoms in the germanium clusters still keep the ferromagnetic coupling, and how does the total magnetic moment of the clusters evolve with added Fe atoms? For Fe_2Ge_n, only Qiang et al.[38] investigated the stable structures and magnetic moments of small-sized neutral Fe_2Ge_n clusters with n = 1−8 using DFT calculations.

Although many theoretical studies have predicted intriguing properties, such as magnetism through metal doping into the semiconductor clusters,[2] to our knowledge, no direct experimental measurement on the magnetism of metal-doped semiconductor clusters has reported in the literature. In this article, we report an extensive search for the lowest-energy structures of the anionic and neutral Fe_2Ge_n (n = 3−12) clusters using an ab initio based genetic algorithm. The electronic properties and magnetic properties of the identified lowest-energy clusters are analyzed by taking advantage of the measured photoelectron spectra. Our results show that double Fe atom doped germanium clusters can maintain high magnetic moments to avoid the magnetic quenching behavior typically seen in single Fe atom doped germanium clusters.

2. EXPERIMENTAL AND THEORETICAL METHODS

2.1. Experimental Methods. The experiments were carried out using a home-built apparatus consisting of a laser vaporization cluster source, a time-of-flight mass spectrometer, and a magnetic-bottle photoelectron spectrometer, which has been described before.[39] The Fe−Ge cluster anions were generated in the laser vaporization source by laser ablation of a rotating and translating disk target (13 mm diameter, Fe:Ge mole ratio 1:2) with the second harmonic (532 nm) light pulses from a Nd:YAG laser (Continuum Surelite II-10), while helium gas with ∼4 atm backing pressure was allowed to expand through a pulsed valve (General Valve Series 9) into the source to cool the formed clusters. The generated cluster anions were mass-analyzed with a time-of-flight mass spectrometer. The cluster anions of interest were size-selected with a mass gate and decelerated by a momentum decelerator before being crossed with the laser beam of another Nd: YAG laser (Continuum Surelite II-10, 266 nm) at the photodetachment region. The photoelectrons were energy-analyzed by a magnetic-bottle photoelectron spectrometer. The resolution of the magnetic-bottle photoelectron spectrometer was about 40 meV at electron kinetic energy of 1 eV. The photoelectron spectra were calibrated with the spectra of Cu^- and Au^- ions taken at similar conditions.

2.2. Theoretical Methods. The low-energy structures of the Ge−Fe alloy clusters were globally searched using our own comprehensive genetic algorithm (CGA) code[40] incorporated with DFT calculations (CGA-DFT). The more details of CGA can be found in a recent review article.[40] As one of the most widely adopted global optimization algorithms, GA and its variations have been intensively used in cluster science.[41,42] The validity and efficiency of the present CGA-DFT scheme have been well demonstrated in our previous studies on alloy clusters such as Na−Si,[43] V−Si,[35,44] Pt−Sn,[45] Au−Ag,[46] and Si−B[47] clusters.

All cluster isomers were fully relaxed based on DFT optimization (without any symmetry constraint) with double numerical basis including p-polarization function (DNP) and the Perdew−Burke−Enzerhof (PBE) functional within the generalized gradient approximation[48] (GGA). Self-consistent calculations were done with a convergence criterion of 10^{-6} hartree on the total energy and real-space orbital cutoff of 6 Å. The structures were fully optimized with a convergence criterion of 0.002 hartree/Å on the forces. Many spin multiplicities were considered to account for magnetic behavior of the Fe atom with partially filled 3d orbital. All computations were done using the program DMol^3 7.0.[49,50]

To ensure credibility of the present DFT methodology, we have used Fe_2 and Ge_2 dimers as well as bulk solids of Fe and Ge as benchmark systems. The Fe_2 dimer has a 3 μ_B magnetic moment on each Fe atom, consistent with the previous ab initio calculation[51,52] and also in good agreement with the experimental value of (3.3 ± 0.5) μ_B.[53] The calculated Fe−Fe bond length is 2.04 Å, in excellent agreement with the experimental value of 2.02 ± 0.02 Å.[54] Similarly, the theoretical Ge−Ge bond length of 2.43 Å is nearly the same as 2.44 Å from experiment.[55] From our DFT calculations, the vibrational frequencies of Fe_2 and Ge_2 dimers are 325 and 263 cm^{-1}, which compared reasonably well with experimental data of 300 ± 15[56] and 286 ± 5[57] cm^{-1}, respectively. The calculated binding energies of Fe_2 and Ge_2 dimers are 0.86 and 1.46 eV/atom, also in line with the experimental data of 0.82 ± 0.3[58] and 1.32 eV/

DOI: 10.1021/acs.jpcc.7b00943
J. Phys. Chem. C 2017, 121, 7037−7046

atom,[59] respectively. In addition, the equilibrium lattice constants of iron (in body-centered cubic structure) and germanium (in diamond structure) solids are 2.858 and 5.785 Å, respectively, and the cohesive energies for Fe and Ge solids are 4.29 and 3.27 eV/atom, respectively. For comparison, the experimental lattice constants are 2.866 and 5.657 Å for Fe and Ge solids,[60] and the corresponding cohesive energies[61] are 4.28 and 3.85 eV/atom, respectively. Overall, our PBE/DNP scheme can describe the structural and bonding properties of Fe and Ge systems quite well.

3. RESULTS AND DISCUSSION

3.1. Anionic $Fe_2Ge_n^-$ (n = 3−12) Clusters. *3.1.1. Growth Behavior of $Fe_2Ge_n^-$ (n = 3−12) Clusters.* The lowest-energy structures of $Fe_2Ge_n^-$ (n = 3−12) clusters obtained from CGA-DFT search are displayed in Figure 1, along with some important structural isomers for discussion. The ground-state structure of $Fe_2Ge_3^-$ with spin multiplicity of sextet is of C_s symmetry with one Fe atom capped on the quadrangle. The average Ge−Ge and Fe−Ge bond lengths of the quadrangle are 2.59 and 2.35 Å, respectively, while the Fe−Fe bond length is 2.71 Å. For the $Fe_2Ge_4^-$ cluster, its ground-state structure of octet spin state is a face-capped square bipyramid with C_{2v} symmetry (4a in Figure 1). The metastable structure of isomer 4b (octet) with C_s symmetry resembles the ground-state structure, while its energy is only 0.01 eV higher than that of 4a. The Fe−Fe bond length of the ground-state structure is 2.42 Å, while it is 2.44 Å in the metastable 4b structure. Isomer 4c, with spin multiplicity of sextet, is 0.44 eV higher than 4a in energy, and its structure looks like a "boat" based on the triangular pyramid.

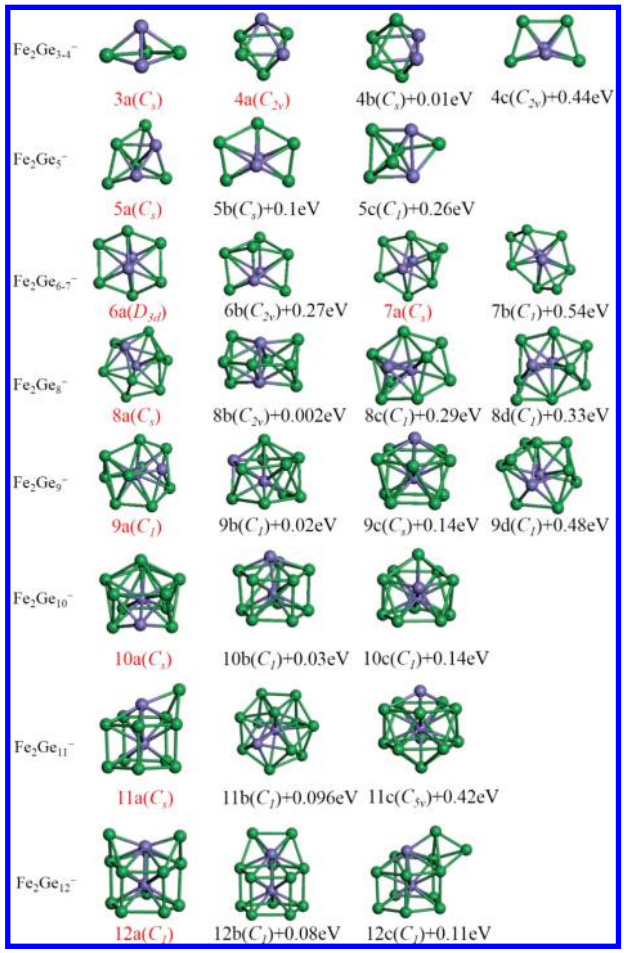

Figure 1. Low-energy structures of $Fe_2Ge_n^-$ (n = 3−12) clusters. For each cluster size, several low-energy isomers marked as b, c, and d plus energy difference relative to the lowest-energy one (marked as a). The symmetries are given in parentheses. Green and purple balls represent Ge and Fe atoms, respectively.

For $Fe_2Ge_5^-$, the ground-state structure with spin multiplicity of sextet is based on a triangle bipyramid with two Ge atoms caped on its two faces. The metastable isomer 5b (sextet) is an unclosed pentagonal bipyramid capped with two Fe atoms and lies 0.1 eV higher in energy. 5c (doublet) isomer is a face-capped square bipyramid with one Ge atom decorated on one face, while its energy is 0.26 eV higher than that of the ground-state structure. The lowest-energy structure of $Fe_2Ge_6^-$ (sextet) has D_{3d} symmetry and is a hexagonal bipyramid with two Fe atoms on the top sites of the pyramid separately. The metastable isomer 6b (sextet), which looks like one Ge atom capping on another face of the 5c structure, is 0.27 eV higher in energy with C_{2v} symmetry.

For $Fe_2Ge_7^-$, the ground-state structure 7a with spin multiplicity of sextet is a distorted hexagonal bipyramid with one Ge atom decorated on it, having a C_s symmetry, while the isomer 7b (doublet) is based on a pentagonal bipyramid with two Ge atoms capped on two faces separately. Its total energy is 0.54 eV higher than that of 7a configuration. For $Fe_2Ge_8^-$, the lowest-energy structure 8a (sextet) and its isomers 8c and 8d are all based on the pentagonal bipyramid with the added three atoms decorated on different faces, while the structure 8b of sextet state with C_{2v} symmetry is two quadrilateral bipyramids side-by-side, with the added one Ge atom decorated on the Fe−Fe bond side. The 8a and 8b isomers of $Fe_2Ge_8^-$ differ by only 0.002 eV in energy. 8c and 8d are 0.29 and 0.33 eV higher in energy compared to 8a, respectively.

Among the low-energy isomers of $Fe_2Ge_9^-$ cluster (all with spin multiplicity of sextet), 9a is based on pentagonal bipyramid, which can be built upon the 8a configuration by adding an extra Ge atom. The metastable isomers 9b and 9c are cagelike structures with one Fe atom in the cage center. The difference between 9b and 9c is the placement of the added one Fe atom. In 9b, the Fe atom makes up the pentagon on top with other four Ge atoms, which also leads to an open quadrangle on the bottom; while in 9c, the Fe atom on the vertex of the pentagon constitutes a closed cage structure with C_s symmetry. The isomer 9d can be viewed as capping one Ge atom on the configuration of 8a. Compared with the ground state, the energy difference is 0.02, 0.14, and 0.48 eV for 9b, 9c, and 9d, respectively.

For $Fe_2Ge_{10}^-$, the most stable structure is a distorted icosahedron with an endohedral Fe atom (sextet). The metastable isomer (10b of quartet) is an Fe-center pentagonal prism capped with the remaining one Fe atom on a vertex, whose energy is 0.03 eV higher than that of the ground-state structure. The isomer 10c (sextet) is 0.14 eV higher than 10a, and its Fe-center cagelike structure can be described as one pentagonal pyramid on the bottom of a hexagonal pyramid. In $Fe_2Ge_{11}^-$, the lowest-energy structure with C_s symmetry (11a of quartet) is obtained by adding one Ge atom on 10b. Its total energy is 0.096 eV lower than that of isomer 11b (quartet). The structure of 11b can be viewed as a pentagonal pyramid and hexangular pyramid fusing together to construct an open cagelike configuration with one interior Fe atom. Note that the

DOI: 10.1021/acs.jpcc.7b00943
J. Phys. Chem. C 2017, 121, 7037−7046

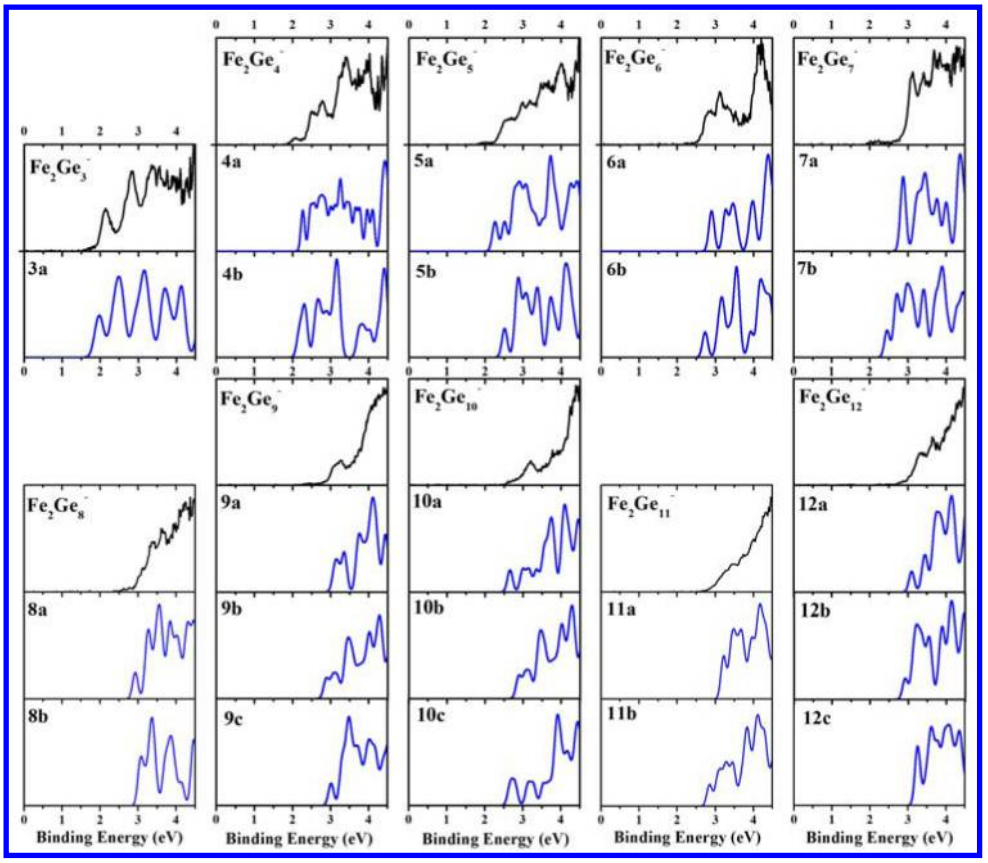

Figure 2. Photoelectron spectra of low-lying isomers of $Fe_2Ge_n^-$ (n = 3−12) from experiment (upper panels in black) and theory (lower panels in blue). The simulations were conducted by fitting the distribution of the transition lines with unit-area Gaussian functions of 0.07 eV.

icosahedron isomer 11c (octet) is 0.42 eV higher in energy than the ground-state isomer 11a.

The ground-state geometry of $Fe_2Ge_{12}^-$ (with spin multiplicity of quartet) is obtained by adding two Ge atoms on the top of 10b separately. It is 0.08 eV lower than the isomer 12b (doublet) with two closer adding Ge atoms. While the structure of 12c (quartet) by adding two Ge atoms on one side is 0.11 eV higher than the ground-state structure. In general, all these $Fe_2Ge_{12}^-$ isomers are based on an Fe-center pentagonal prism with one Fe atom on top like a cap.

Overall, in the low-lying structures of $Fe_2Ge_n^-$ (n = 3−12) clusters, Fe atoms tend to bond with each other instead of being separated by Ge atoms because the Fe−Fe bond is stronger than the Fe−Ge bond. For all $Fe_2Ge_n^-$ clusters considered, the lengths of Fe−Fe bonds are in the range of 2.271−2.441 Å, moderately shorter than bond lengths of Fe−Ge (2.351−2.766 Å) and Ge−Ge (2.510−2.797 Å). The smaller $Fe_2Ge_n^-$ clusters with n = 4−8 adopt bipyramid-based structures, while one interior Fe atom starts to appear from n = 9. The spin-multiplicity for the ground-state structures of $Fe_2Ge_n^-$ are mostly sextet, except for $Fe_2Ge_4^-$ with octet and $Fe_2Ge_{11}^-$ and $Fe_2Ge_{12}^-$ with quartet.

3.1.2. Photoelectron Spectra from Experiment and Theory. The photoelectron spectra of $Fe_2Ge_n^-$ (n = 3−12) measured at 266 nm photons are presented in the upper panels (black curves) of Figure 2, and the lower panels (blue curves) are the corresponding spectra from theoretical simulations. In each experimental spectrum, the vertical detachment energy (VDE) denotes the transition from the ground electronic state of the anionic cluster to the same structure of the neutral one, and the adiabatic detachment energy (ADE) is the difference in total energy between the anionic cluster and the neutral cluster in their optimized geometries. The other peaks with higher binding energy denote transitions to excited electronic states of the neutral clusters. On experimental photoelectron spectrum, one can determine the VDE from the peak maximum of the first feature and ADE from the leading edge of the first feature. The theoretical VDEs and ADEs of these low-lying isomers are summarized in Table 1 along with the experimental values for comparison.

As shown in Figure 2, the spectrum of $Fe_2Ge_3^-$ reveals two relatively sharp peaks at 2.14 and 2.82 eV followed by an extended and congested feature beyond 3.3 eV. The theoretical VDE (1.92 eV) of the lowest-energy structure is slightly lower than the experimental value (2.14 eV). The overall simulated spectrum is in good agreement with the experimental spectrum, leaving only a small shift of the simulated spectrum to lower binding energy. In the measured spectrum of $Fe_2Ge_4^-$, five peaks are seen at 2.07, 2.50, 2.78, 3.42, and 4.02 eV. The isomers 4a and 4b have very small energy difference, and their computed VDEs are 2.27 eV. The simulated spectrum for the ground-state structure (4a) coincides well with the experimental spectrum, but the contribution from isomer 4b cannot be ruled out, because 4a and 4b are nearly degenerate in energy, even after including zero-point correction by using Gaussian 09[62] (see Table S1). For $Fe_2Ge_5^-$, a total of five peaks, 2.50, 2.98, 3.17, 3.61, and 4.02 eV, are observed. The theoretical VDE is 2.26 eV, and the non-negligible shoulders appearing first in the simulated curve results in a VDE that is smaller than the experimental VDE. The metastable structure (5b), which is

DOI: 10.1021/acs.jpcc.7b00943
J. Phys. Chem. C 2017, 121, 7037−7046

Table 1. VDEs and ADEs of the Isomers for $Fe_2Ge_n^-$ (n = 3−12) Clusters Estimated from Experimental Photoelectron Spectra and Theoretical Calculation

		VDEs (eV)		ADEs (eV)	
isomer		theo.	exptl.	theo.	exptl.
$Fe_2Ge_3^-$	3a	1.92	2.14 ± 0.08	1.82	1.89 ± 0.08
$Fe_2Ge_4^-$	4a	2.27	2.07 ± 0.08	2.18	1.77 ± 0.08
	4b	2.18		2.10	
	4c	2.00		1.91	
$Fe_2Ge_5^-$	5a	2.26	2.50 ± 0.08	2.16	2.25 ± 0.08
	5b	2.51		2.41	
$Fe_2Ge_6^-$	6a	2.90	2.82 ± 0.08	2.48	2.56 ± 0.08
	6b	2.73		2.48	
$Fe_2Ge_7^-$	7a	2.86	3.13 ± 0.08	2.80	2.90 ± 0.08
	7b	2.46		2.31	
$Fe_2Ge_8^-$	8a	2.93	3.11 ± 0.08	2.84	2.85 ± 0.08
	8b	3.06		2.93	
	8c	2.87		2.69	
	8d	2.89		2.77	
$Fe_2Ge_9^-$	9a	3.11	3.11 ± 0.08	2.88	2.85 ± 0.08
	9b	2.88		2.79	
	9c	3.01		2.76	
	9d	2.87		2.76	
$Fe_2Ge_{10}^-$	10a	2.66	3.20 ± 0.08	2.50	2.82 ± 0.08
	10b	3.07		2.90	
	10c	2.67		2.76	
$Fe_2Ge_{11}^-$	11a	3.21	3.30 ± 0.08	3.06	2.83 ± 0.08
	11b	2.85		2.71	
	11c	2.88		2.39	
$Fe_2Ge_{12}^-$	12a	3.10	3.37 ± 0.08	3.25	2.99 ± 0.08
	12b	2.92		2.73	
	12c	3.25		3.11	

higher in energy than 5a by 0.1 eV, has theoretical VDE of 2.51 eV, and its simulated photoelectron spectrum is consistent with the experimental one. Hence, both isomers likely coexist in the cluster beam, and both contribute to the experimental spectrum.

In the spectrum of $Fe_2Ge_6^-$, there are three overlapping peaks at 2.82, 3.12, and 3.42 eV, followed by one high peak at 4.20 eV. The calculated VDE is 2.90 eV for the lowest-energy configuration (6a), which is consistent with the experimental value (2.82 eV). The simulated spectrum of isomer 6a also agrees very well with the experimental one. Isomer 6b is much less stable than 6a, and its simulated photoelectron spectrum indicates that it is unlikely to exist in experiment. For $Fe_2Ge_7^-$, its spectrum shows five major peaks at 3.13, 3.42, 3.69, 3.84, and 4.30 eV. The first peak of simulated spectrum is located at 2.86 eV, which is smaller than the experimental value, while the following peaks generally reproduce the experimental features well. For comparison, its isomer 7b with even smaller VDE (2.46 eV) and the simulated photoelectron spectrum does not agree with the experimental one. Therefore, we suggest isomer 7a to be the most probable one observed in experiment.

The experimental spectrum of $Fe_2Ge_8^-$ appears congested and broad, which consists of five peaks centered at 3.11, 3.40, 3.68, 3.94, and 4.18 eV, respectively. The calculated VDEs of two low-lying isomers 8a and 8b are 2.93 and 3.06 eV, respectively. Although the VDE of isomer 8b is closer to the experimental value (3.11 eV) than isomer 8a, 8b may coexist with 8a in the cluster beam, as the simulated photoelectron spectrum of 8a appears to coincide with the experimental spectrum better.

In the spectrum of $Fe_2Ge_9^-$, a low peak arises at 3.11 eV, followed by an intense peak beyond 4.1 eV. The predicted VDE of isomers 9a, 9b, and 9c are 3.11, 2.88, and 3.01 eV, respectively. The energy differences of 9b and 9c with respect to isomer 9a are only about 0.02 and 0.14 eV, respectively. On the basis of the simulated photoelectron spectra in Figure 2, the experimental spectrum of $Fe_2Ge_9^-$ is more likely contributed by a mixture of the three isomers. Similar to $Fe_2Ge_9^-$, the spectrum of $Fe_2Ge_{10}^-$ shows two peaks; one is at 3.20 eV, and the other broad and intense peak is beyond 3.8 eV. The theoretical VDE (2.66 eV) of the ground-state structure 10a is substantially lower than the experimental value. This may be associated with the very weak peak at ∼2.7 eV in the experimental spectrum. The metastable structures, 10b and 10c, are higher in energy than 10a by only 0.03 and 0.14 eV, respectively, and their theoretical VDEs are 3.07 and 2.67 eV. Their simulated spectra appear to contribute to the experimental spectrum as well. Hence, the three low-lying isomers may coexist in the cluster beam.

Only one broad feature is revealed for $Fe_2Ge_{11}^-$. The calculated VDE is 3.21 eV for the lowest-energy isomer 11a, which is reasonably close to the experimental value (3.30 eV). When compared with the experimental spectra, the contribution from metastable isomer 11b cannot be neglected. They are nearly degenerate to coexisting in the experiment. The experimental spectrum of $Fe_2Ge_{12}^-$ is similar to that of $Fe_2Ge_{11}^-$. The energy difference among its isomers is very small. The computed VDEs are 3.10, 2.92, and 3.25 eV for 12a, 12b, and 12c, respectively. The theoretical VDE of isomer 12c is much closer to the experimental value (3.37 eV) than isomer 12a and 12b. The experimental spectrum with less sharp features is likely contributed by the combination of simulated spectra of all three isomers. Thus, all three isomers may coexist in the cluster beam. In general, the experimental spectra of all $Fe_2Ge_n^-$ clusters are reasonably reproduced by the theoretical simulated spectra.

3.1.3. Electronic Properties of $Fe_2Ge_n^-$ (n = 3−12) Clusters in the Ground-State Structures. To further explore the size-dependence of the electronic properties of $Fe_2Ge_n^-$ clusters, the experimental and theoretical VDEs and ADEs as functions of the cluster size are plotted in Figure 3. The experimental VDEs of $Fe_2Ge_n^-$ (n = 3−12) are in the range of 2.07−3.37 eV. It can be seen that the experimental VDE roughly increases with cluster size. The ADE keeps rising from 1.89−2.56 eV for $Fe_2Ge_n^-$ (n = 3−6) clusters, and this trend is slow in the range of 2.90−2.99 eV as the number of Ge atoms increases from 7 to 12. The theoretical VDEs and ADEs are well consistent with those of experiments, except at $Fe_2Ge_{10}^-$. Indeed, the VDE (2.66 eV) of the lowest-lying isomer 10a deviates substantially from the experimental data (3.20 eV); instead, the VDE of the second lowest-lying one (3.07 eV) is very close to the experimental value.

3.2. Neutral Fe_2Ge_n (n = 3−12) Clusters. *3.2.1. Ground-State Structures and Stability of Fe_2Ge_n (n = 3−12) Clusters.* In addition to the geometries of $Fe_2Ge_n^-$ (n = 3−12) anion clusters, we show the ground-state structures of their neutral counterparts in Figure 4. The numbers on-site are the magnetic moment of each Fe atom that will be discussed in the next section. For Fe_2Ge_n ($3 \le n \le 7$), the most stable configurations are nearly the same as the corresponding anionic clusters. For Fe_2Ge_n ($3 \le n \le 5$) clusters, we obtain almost the same

DOI: 10.1021/acs.jpcc.7b00943
J. Phys. Chem. C 2017, 121, 7037−7046

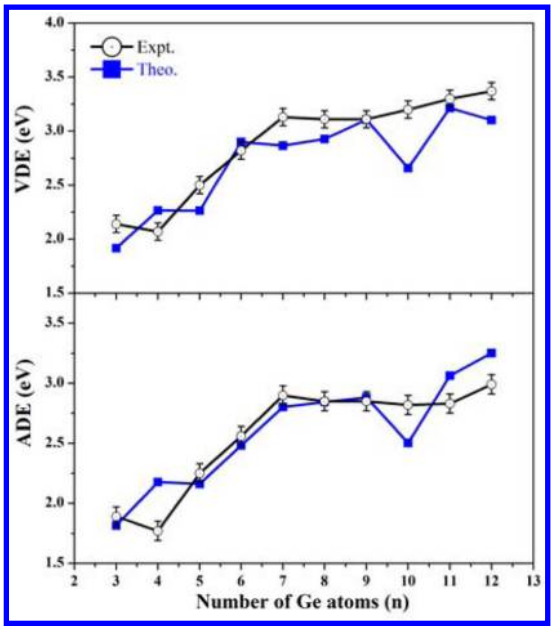

Figure 3. Vertical detachment energies (VDEs) and adiabatic detachment energies (ADEs) of $Fe_2Ge_n^-$ (n = 3−12) clusters. Black circles, experiment; blue squares, theory.

configurations as that reported by Qiang et al.[38] It is worth noting that, for Fe_2Ge_6, they predicted the metastable isomer 6b of $Fe_2Ge_6^-$ anion as the ground-state structure. From our calculations, however, its total energy is 0.31 eV higher than that of the current ground-state structure with D_{3d} symmetry. Similarly, the lowest-energy structures for both Fe_2Ge_7 and Fe_2Ge_8 clusters from our DFT calculation are 0.05 eV lower in energy than the previously reported ones.

In the case of Fe_2Ge_n ($n \geq 8$) clusters, the most stable configurations of the neutral clusters differ from the corresponding anions, but the trend of structural evolution is basically the same, that is, forming polyhedral cagelike structure with one interior Fe atom. For the Fe_2Ge_8 cluster, the skeleton of pentagonal bipyramid resembles that of $Fe_2Ge_8^-$, but with one Fe atom decorated on a different location. For Fe_2Ge_9, a distorted quadrangle on the bottom and a pentagonal bipyramid on the top form an open cagelike structure with one Fe atom in the center, which can be seen as the metastable structure of $Fe_2Ge_{10}^-$ (10b in Figure 1) losing one Ge atom from its bottom. In the case of Fe_2Ge_{10}, it is composed of a pentagonal bipyramid on the top of a quadrangle bipyramid to form an Fe-centered closed cage configuration.

The ground-state structures of Fe_2Ge_{11} and Fe_2Ge_{12} are both based on a hexagonal pyramid and a pentagonal pyramid with one interior Fe atom, while one extra Fe atom capped to form a closed cage structure for the latter structure. In short, for Fe_2Ge_n clusters with $n \geq 10$, the ground-state structures are different from the corresponding anions with skeleton of pentagonal prism, that is, even one extra electron would affect the geometric configurations of Fe_2Ge_n clusters.

To illustrate the structural stability of Fe_2Ge_n (n = 3−12) clusters, we plot the binding energies as a function of size n in Figure 5a. The binding energy per atom gradually increases

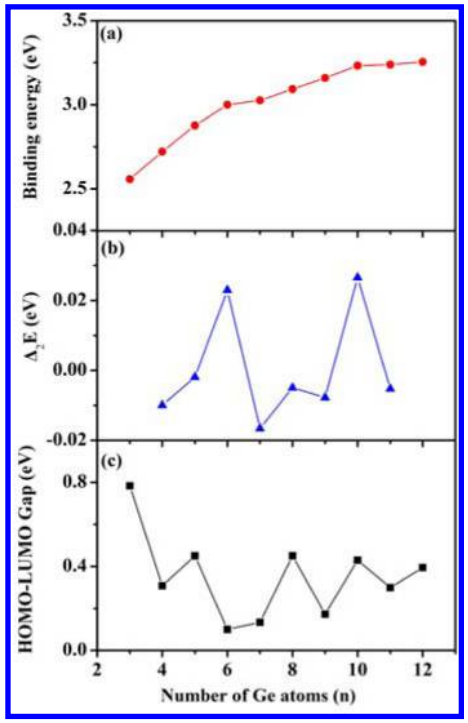

Figure 5. (a) Binding energies, (b) second-order of energy differences of cluster energies defined by $\Delta_2E = E(n+1) + E(n-1) - 2E(n)$, and (c) HOMO−LUMO gaps of neutral Fe_2Ge_n (n = 3−12) clusters.

with growing number of Ge atoms, suggesting that the formation of a cluster is more and more favorable as it becomes bigger. To further examine the relative stability, the second-order energy differences (Δ_2E) are calculated and plotted in Figure 5b. Two distinct peaks at Fe_2Ge_6 and Fe_2Ge_{10} indicate that they are more stable than their neighboring sized clusters. It is also observed that Fe_2Ge_6 and Fe_2Ge_{10} are salient

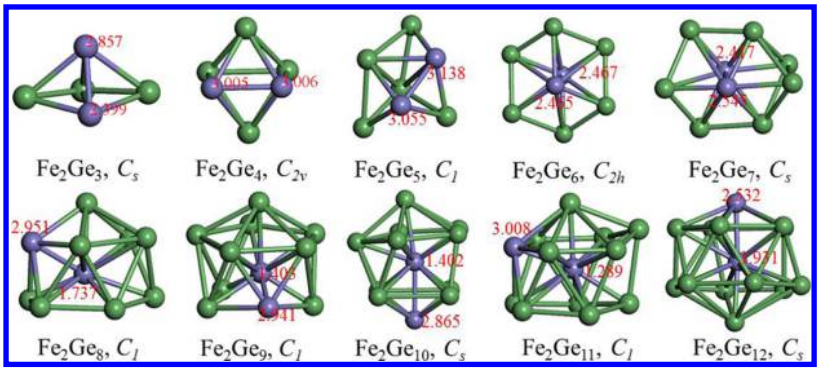

Figure 4. Ground-state structures of neutral Fe_2Ge_n (n = 3−12) clusters and the on-site spin moment in μ_B of iron atoms.

DOI: 10.1021/acs.jpcc.7b00943
J. Phys. Chem. C 2017, 121, 7037−7046

on the curve of binding energy. Thus, we conclude the magic clusters are $n = 6$ and $n = 10$ for Fe_2Ge_n ($3 \le n \le 12$) clusters. The high stability comes from the high symmetry of the cluster structures; for Fe_2Ge_{10}, it is mainly related to the formation of the closed cage structure.

As shown in Figure 5c, the highest occupied molecular orbital−lowest unoccupied molecular orbital (HOMO−LUMO) gaps of Fe_2Ge_n clusters are all less than 1 eV, and it presents two patterns of odd−even oscillation with the exception at $n = 7$, which is related to the structural evolution from hollow to core−shell configuration. Fe_2Ge_6, Fe_2Ge_7, and Fe_2Ge_9 possess relatively smaller gaps compared with their neighbors. We also compare these gap values (0.10−0.78 eV) to those of the pure germanium clusters with the same number of Ge atoms. The gaps of Ge_n ($n = 3$−12) clusters from previous DFT calculations[63] are in the range of 1.2−2.3 eV. Therefore, doping Ge_n clusters with two Fe atoms greatly reduces the HOMO−LUMO gaps. To understand this effect, we examine the partial density of states (PDOS) from the contribution of different orbital components (s, p, and d). Figure 6 gives the PDOS of some representative Fe_2Ge_n

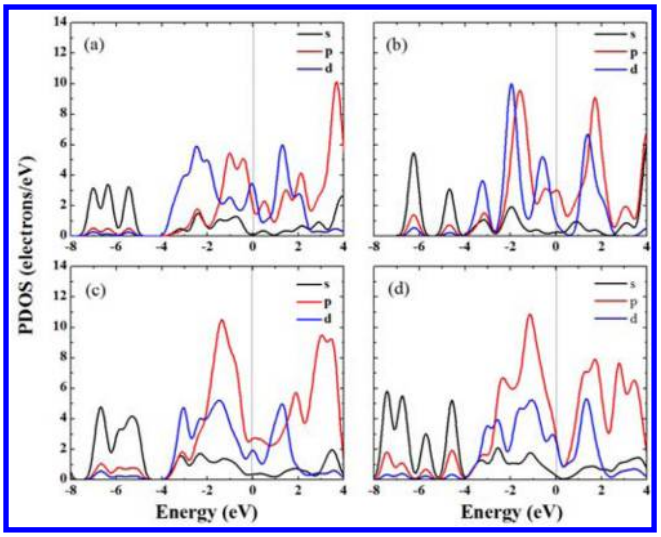

Figure 6. Partial density of states (PDOS) of s, p, and d orbitals for (a) Fe_2Ge_4, (b) Fe_2Ge_6, (c) Fe_2Ge_9, and (d) Fe_2Ge_{11} clusters. The dashed vertical lines indicate the Fermi level.

clusters ($n = 4, 6, 9, 11$). Clearly, the electronic states at the vicinity of the Fermi level originate mainly from p and d states with only very small contribution from s states. Thus, p−d hybridization is responsible for the reduction in the HOMO−LUMO gap upon addition of Fe atoms. The hybridization of Fe d orbital and Ge p orbital also can be visualized intuitively from the frontier molecular orbitals in Figure 7.

3.2.2. Charge Transfer and Magnetic Properties of Fe_2Ge_n ($n = 3$−12) Clusters. On the basis of the optimized geometries of the neutral Fe_2Ge_n clusters, the charge transfer and magnetic moments of these clusters are evaluated via the Mulliken population analysis (MPA), and the results are presented in Table 2. The on-site magnetic moment of two iron atoms are marked in Figure 4. As seen in Table 2, the total spin moments are 4 or 6 μ_B and mainly located on two iron atoms. Obviously, Fe_2Ge_4 and Fe_2Ge_5 own a larger magnetic moment of 6 μ_B, which is triple that of single Fe atom doping.[28] Also for Fe_2Ge_9, the spin moment rises up to 4 μ_B compared to 0 μ_B of $FeGe_9$.[29] The on-site magnetic moments of the two iron atoms exhibit

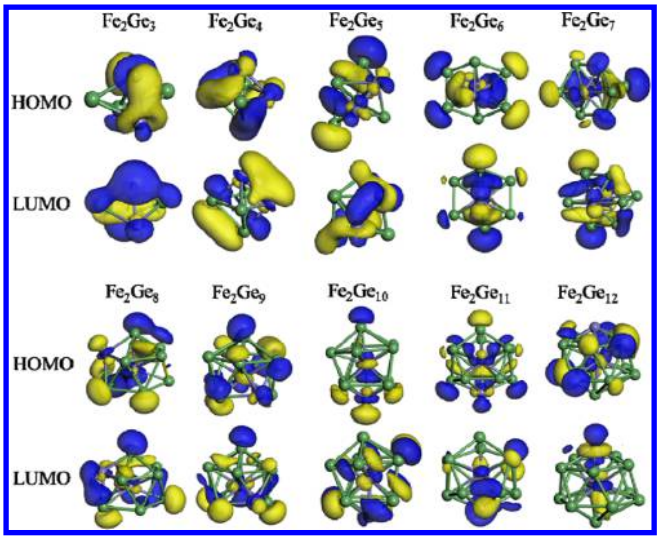

Figure 7. HOMO and LUMO orbitals of the neutral Fe_2Ge_n ($n = 3$−12) clusters with ground-state structures.

Table 2. On-Site and Total Spin Moments (μ_B) of Fe atoms in Fe_2Ge_n ($n = 3$−12) Clusters from Milliken Population Analyses (MPA) and the On-Site Charges of Fe Atoms

	spin moment (μ_B)			MPA charge (|e|)	
cluster	Fe1	Fe2	total	Fe1	Fe2
Fe_2Ge_3	2.399	2.857	4	0.273	0.310
Fe_2Ge_4	3.005	3.006	6	0.331	0.331
Fe_2Ge_5	3.055	3.318	6	0.315	0.312
Fe_2Ge_6	2.467	2.465	4	0.378	0.379
Fe_2Ge_7	2.545	2.417	4	0.421	0.333
Fe_2Ge_8	2.951	1.737	4	0.440	0.281
Fe_2Ge_9	1.403	2.941	4	0.213	0.468
Fe_2Ge_{10}	1.402	2.865	4	0.271	0.331
Fe_2Ge_{11}	1.289	3.008	4	0.327	0.438
Fe_2Ge_{12}	1.931	2.532	4	0.383	0.401

ferromagnetic coupling. The antiferromagnetic coupling between Fe atom and Ge atom is observed, which was also discovered in single Fe atom doped Ge_n clusters.[28,29] Interestingly, when the cagelike configuration is formed, i.e., $n \ge 8$, the spin moment of Fe atom on the surface is obviously larger than that of the interior Fe atom. What causes the difference of the on-site magnetic moment? The reason will be discussed below.

As we know, the pure Fe_2 dimer has a spin moment of 3 μ_B per atom.[51−53] When the Fe_2 dimer is doped into a nonmagnetic germanium cluster, the on-site magnetic moments become dependent on the coordination environment. The change of the magnetic moments on Fe atoms mainly stems from the charge transfer between the Fe atoms and the host Ge_n cluster. We show the on-site charge of two iron atoms in Table 2 and observe that the Fe atoms act as electron donors in all investigated Fe_2Ge_n ($n = 3$−12) clusters. To understand further, we list the charge and spin on valence orbitals of two Fe atoms and each Ge atom separately in Table S2. The configurations of valence electrons for free atom are $3d^64s^2$ for Fe and $4s^24p^2$ for Ge. For all Fe_2Ge_n clusters considered here, the 3d state gains extra electrons from 4s states, and some electrons transfer to 4p state. This indicates that internal s−pd hybridization occurs on the iron atoms. It can be clearly seen

DOI: 10.1021/acs.jpcc.7b00943
J. Phys. Chem. C 2017, 121, 7037−7046

that the spin moment on iron atom mainly comes from its 3d state (see details in Table S2), and the extra electrons gained by the 3d state will determine the variations of spin moment on it, i.e., the fewer electrons it gains, the larger spin moment it has. For example, for Fe_2Ge_4 and Fe_2Ge_5 clusters with relatively large on-site spin moments of iron atoms, the 3d states of two iron atoms gain about 0.78 and 0.78 e for the former, 0.74 and 0.71 e for the latter, respectively, which are relatively less than the others (~0.9 e). This can be related to the core−shell clusters ($n \geq 8$), i.e., the Fe atom on the surface is most likely to gain fewer electrons for its 3d state which results in a larger magnetic moment on it. This mainly accounts for its relative larger on-site magnetic moment (~3 μ_B).

Besides the internal charge transfer of Fe atom, there is also a significant internal charge transfer of Ge atom between 4s and 4p states (4s states own about 1.8 e and 4p states have about 2.2 e, as shown in Table S2) as well as the charge transfer between Fe and Ge atoms. The total magnetic moment of Fe_2Ge_4 or Fe_2Ge_5 (6 μ_B) is larger than that of the other clusters (4 μ_B), which is also related to the variations of induced magnetic moments on Ge atoms. Thus, there should be a correspondence between the charge transfer and magnetic moment. The above detailed discussions suggest that the charge transfer and hybridization between Fe (4s, 3d) and Ge (4s, 4p) states can explain the magnetic moments variation in different sizes of the doped clusters.

3.2.3. Frontier Molecular Orbitals of Fe_2Ge_n (n = 3−12) Clusters. To further understand the interaction between Fe atoms and Ge atoms in the Fe_2Ge_n clusters, we plot the HOMOs and the LUMOs in Figure 6. It can be seen that the frontier molecular orbitals mainly originate from Fe d-orbital and Ge p-orbital. The Fe_2Ge_6 cluster displays distinct p−d hybridization, thus possessing high stability. For $n \leq 7$, the electron distributions are almost identical for the two Fe atoms, that is, the interaction from Ge atoms to each Fe atom are almost equal, which may be the main reason for the comparable magnetic moment on each Fe atom. In the case of $n \geq 8$, cagelike configurations begin to form and the electron distributions are different for two Fe atoms, meaning that different interactions from Ge atoms will result in different spin moments on two Fe atoms.

Overall, the HOMO and LUMO are composed of Fe d states mixed with Ge p states. The unique p−d hybridization is responsible for the reduced HOMO−LUMO gap of Fe_2Ge_n (n = 3−12) clusters with regard to the pure Ge_n clusters and for the robust magnetic moments of the iron-doped clusters.

4. CONCLUSION

In summary, we systematically investigate the structural and electronic properties of double Fe atom doped semiconductor clusters Ge_n in the size range of $3 \leq n \leq 12$. The theoretically simulated photoelectron spectra of $Fe_2Ge_n^-$ anion clusters largely reproduce the experimental spectrum. In the exceptional case of $Fe_2Ge_{10}^-$, the difference between experiment and theory may be ascribed to the coexistence of two energetically degenerate isomers. Starting from $n \geq 8$, the ground-state structures of neutral Fe_2Ge_n clusters are different from those of the corresponding anions, indicating that one extra electron on the Fe_2Ge_n clusters can significantly affect the lowest-energy structures. We have also searched the most stable structures of neutral Fe_2Ge_n clusters and computed their electronic and magnetic properties. We find that their spin moments are generally higher than those of the $FeGe_n$ clusters. It is noteworthy that the double Fe atom doped germanium clusters are in stark contrast to the quenched magnetic moment for single Fe atom doped germanium clusters. In particular, Fe_2Ge_4 and Fe_2Ge_5 have magnetic moments of 6 μ_B, remarkably higher than the magnetic moments of other sizes. Interestingly, the magnetic coupling between the two Fe atoms in all the germanium clusters considered is ferromagnetic, while antiferromagnetic interactions are also found between Fe dopants and some Ge atoms. The present results give important indications of changing the magnetic behavior of TM-doped semiconductor clusters by changing the number of TM dopant atoms.

■ ASSOCIATED CONTENT

Supporting Information

The Supporting Information is available free of charge on the ACS Publications website at DOI: 10.1021/acs.jpcc.7b00943.

Zero-point correction of the low-energy structures for $Fe_2Ge_n^-$ and the charge and spin of each atom for neutral clusters discussed in this study (PDF)

■ AUTHOR INFORMATION

Corresponding Authors

*E-mail: zhaojj@dlut.edu.cn.
*E-mail: xuhong@iccas.ac.cn.
*E-mail: xzeng1@unl.edu.

ORCID

Ji-Jun Zhao: 0000-0002-0842-1075
Wei-Jun Zheng: 0000-0002-9136-2693
Xiao Cheng Zeng: 0000-0003-4672-8585

Notes

The authors declare no competing financial interest.

■ ACKNOWLEDGMENTS

This work was supported by the National Natural Science Foundation of China (11574040, 21103202, 11604039) and the Fundamental Research Funds for the Central Universities of China (DUT15RC(3)099, DUT16-LAB01). X.-C.Z. was supported by a Qian-ren B (One Thousand Talent Plan B) summer research fund from USTC and by a State Key R&D Fund of China (2016YFA0200604) to USTC.

■ REFERENCES

(1) Dietl, T. A Ten-Year Perspective on Dilute Magnetic Semiconductors and Oxides. *Nat. Mater.* **2010**, *9*, 965−974.

(2) (a) Zhao, J. J.; Huang, X. M.; Jin, P.; Chen, Z. F. Magnetic Properties of Atomic Clusters and Endohedral Metallofullerenes. *Coord. Chem. Rev.* **2015**, *289-290*, 315−340. (b) Wang, L. M.; Pal, R.; Huang, W.; Zeng, X. C.; Wang, L. S. Tuning the electronic properties of the golden buckyball by endohedral doping: M@Au16- (M = Ag, Zn, In). *J. Chem. Phys.* **2009**, *130*, 051101. (c) Pal, R.; Wang, L. M.; Huang, W.; Wang, L. S.; Zeng, X. C. Structural Evolution of Doped Gold Clusters: MAu_x^- (M = Si, Ge, Sn; x = 5−8). *J. Am. Chem. Soc.* **2009**, *131*, 3396−3404. (d) Wang, L. M.; Bai, J.; Lechtken, A.; Huang, W.; Schooss, D.; Kappes, M. M.; Zeng, X. C.; Wang, L. S. Magnetic Doping of the Golden Cage Cluster: $M@Au_{16}^-$ (M = Fe, Co, Ni). *Phys. Rev. B: Condens. Matter Mater. Phys.* **2009**, *79*, 033413.

(3) Erwin, S. C.; Zu, L.; Haftel, M. I.; Efros, A. L.; Kennedy, T. A.; Norris, D. J. Doping Semiconductor Nanocrystals. *Nature* **2005**, *436*, 91−94.

(4) Palyanov, Y. N.; Kupriyanov, I. N.; Borzdov, Y. M.; Surovtsev, N. V. Germanium: A New Catalyst for Diamond Synthesis and a New Optically Active Impurity in Diamond. *Sci. Rep.* **2015**, *5*, 14789.

DOI: 10.1021/acs.jpcc.7b00943
J. Phys. Chem. C 2017, 121, 7037−7046

(5) Pillarisetty, R. Academic and Industry Research Progress in Germanium Nanodevices. *Nature* **2011**, *479*, 324−328.
(6) Wang, J.-Q.; Stegmaier, S.; Fässler, T. F. $[Co@Ge_{10}]^{3-}$: An Intermetalloid Cluster with Archimedean Pentagonal Prismatic Structure. *Angew. Chem.* **2009**, *121*, 2032−2036.
(7) Zhou, B.; Denning, M. S.; Kays, D. L.; Goicoechea, J. M. Synthesis and Isolation of $[Fe@Ge_{10}]^{3-}$: A Pentagonal Prismatic Zintl Ion Cage Encapsulating an Interstitial Iron Atom. *J. Am. Chem. Soc.* **2009**, *131*, 2802−2803.
(8) Neukermans, S.; Wang, X.; Veldeman, N.; Janssens, E.; Silverans, R. E.; Lievens, P. Mass Spectrometric Stability Study of Binary MS_n Clusters (S = Si, Ge, Sn, Pb, and M = Cr, Mn, Cu, Zn). *Int. J. Mass Spectrom.* **2006**, *252*, 145−150.
(9) Furuse, S.; Koyasu, K.; Atobe, J.; Nakajima, A. Experimental and Theoretical Characterization of MSi_{16}^-, MGe_{16}^-, MSn_{16}^-, and MPb_{16}^- (M = Ti, Zr, and Hf): The Role of Cage Aromaticity. *J. Chem. Phys.* **2008**, *129*, 064311.
(10) Atobe, J.; Koyasu, K.; Furuse, S.; Nakajima, A. Anion Photoelectron Spectroscopy of Germanium and Tin Clusters Containing a Transition-or Lanthanide-Metal Atom; MGe_n^-(n = 8−20) and MSn_n^-(n = 15−17)(M = Sc−V, Y−Nb, and Lu−Ta). *Phys. Chem. Chem. Phys.* **2012**, *14*, 9403−9410.
(11) Jin, Y. Y.; Lu, S. J.; Hermann, A.; Kuang, X. Y.; Zhang, C.; Lu, C. Z.; Xu, H. G.; Zheng, W. J. Probing the Structural Evolution of Ruthenium Doped Germanium Clusters: Photoelectron Spectroscopy and Density Functional Theory Calculations. *Sci. Rep.* **2016**, *6*, 30116.
(12) Lu, S.-J.; Hu, L.-R.; Xu, X.-L.; Xu, H.-G.; Chen, H.; Zheng, W.-J. Transition from Exohedral to Endohedral Structures of $AuGe_n^-$(n = 2−12) Clusters: Photoelectron Spectroscopy and Ab Initio Calculations. *Phys. Chem. Chem. Phys.* **2016**, *18*, 20321.
(13) Deng, X.-J.; Kong, X.-Y.; Xu, X.-L.; Xu, H.-G.; Zheng, W.-J. Photoelectron Spectroscopy and Density Functional Calculations of $TiGe_n^-$(n = 7−12) Clusters. *Chin. J. Chem. Phys.* **2016**, *29*, 123−128.
(14) Deng, X.-J.; Kong, X.-Y.; Xu, H.-G.; Xu, X.-L.; Feng, G.; Zheng, W.-J. Photoelectron Spectroscopy and Density Functional Calculations of VGe_n^- (n = 3−12) Clusters. *J. Phys. Chem. C* **2015**, *119*, 11048−11055.
(15) Deng, X. J.; Kong, X. Y.; Xu, X. L.; Xu, H. G.; Zheng, W. J. Structural and Magnetic Properties of $CoGe_n^-$(n = 2−11) Clusters: Photoelectron Spectroscopy and Density Functional Calculations. *ChemPhysChem* **2014**, *15*, 3987−3993.
(16) Deng, X.-J.; Kong, X.-Y.; Xu, X.-L.; Xu, H.-G.; Zheng, W.-J. Structural and Bonding Properties of Small $TiGe_n^-$ (n = 2−6) Clusters: Photoelectron Spectroscopy and Density Functional Calculations. *RSC Adv.* **2014**, *4*, 25963−25968.
(17) Wang, J.; Han, J.-G. Geometries and Electronic Properties of the Tungsten-Doped Germanium Clusters: WGe_n (n = 1−17). *J. Phys. Chem. A* **2006**, *110*, 12670−12677.
(18) Tai, T. B.; Nguyen, M. T. Enhanced Stability by Three-Dimensional Aromaticity of Endohedrally Doped Clusters $X_{10}M^{0/-}$ with X = Ge, Sn, Pb and M = Cu, Ag, Au. *J. Phys. Chem. A* **2011**, *115*, 9993−9999.
(19) Bandyopadhyay, D.; Sen, P. Density Functional Investigation of Structure and Stability of Gen and Genni (N = 1−20) Clusters: Validity of the Electron Counting Rule. *J. Phys. Chem. A* **2010**, *114*, 1835−1842.
(20) Wang, J.; Han, J.-G. A Computational Investigation of Copper-Doped Germanium and Germanium Clusters by the Density-Functional Theory. *J. Chem. Phys.* **2005**, *123*, 244303.
(21) Wang, J. G.; Ma, L.; Zhao, J. J.; Wang, G. H. Structural Growth Sequences and Electronic Properties of Manganese-Doped Germanium Clusters: $MnGe_n$ (n = 2−15). *J. Phys.: Condens. Matter* **2008**, *20*, 335223.
(22) Kapila, N.; Jindal, V. K.; Sharma, H. Structural, Electronic and Magnetic Properties of Mn, Co, Ni in Ge_n for (n = 1−13). *Phys. B* **2011**, *406*, 4612−4619.
(23) Kapila, N.; Garg, I.; Jindal, V. K.; Sharma, H. First Principle Investigation into Structural Growth and Magnetic Properties in Ge_nCr Clusters for n = 1−13. *J. Magn. Magn. Mater.* **2012**, *324*, 2885−2893.
(24) Pavlyukh, Y.; Hübner, W. Nonlinear Mie Scattering from Spherical Particles. *Phys. Rev. B: Condens. Matter Mater. Phys.* **2004**, *70*, 245434.
(25) Li, J. R.; Wang, G. H.; Yao, C. H.; Mu, Y. W.; Wan, J. G.; Han, M. Structures and Magnetic Properties of Si_nMn(n = 1−15) Clusters. *J. Chem. Phys.* **2009**, *130*, 164514.
(26) Wang, J. G.; Zhao, J. J.; Ma, L.; Wang, B. L.; Wang, G. H. Structure and Magnetic Properties of Cobalt Doped Si_n (n = 2−14) Clusters. *Phys. Lett. A* **2007**, *367*, 335−344.
(27) Tang, C. M.; Liu, M. Y.; Zhu, W. H.; Deng, K. M. Probing the Geometric, Optical, and Magnetic Properties of 3d Transition-Metal Endohedral $Ge_{12}M$ (M = Sc−Ni) Clusters. *Comput. Theor. Chem.* **2011**, *969*, 56−60.
(28) Zhao, W. J.; Yang, Z.; Yan, Y. L.; Lei, X. L.; Ge, G. X.; Wang, Q. L.; Luo, Y. H. Ground-State Structures and Magnetism of Ge_nFe (*n* = 1−8) Clusters: The Density Functional Investigations. *Acta. Phys. Sin.-Chin. Ed.* **2007**, *56*, 2596−2602.
(29) Zhao, W. J.; Wang, Y. X. Geometries, Stabilities, and Electronic Properties of $FeGe_n$ (n = 9−16) Clusters: Density-Functional Theory Investigations. *Chem. Phys.* **2008**, *352*, 291−296.
(30) Palagin, D.; Teufl, T.; Reuter, K. Multidoping of Si Cages: High Spin States Beyond the Single-Dopant Septet Limit. *J. Phys. Chem. C* **2013**, *117*, 16182−16186.
(31) Ma, Q.-M.; Xie, Z.; Liu, Y.; Li, Y.-C. The Structures, Binding Energies and Magnetic Moments of Cr−C Clusters. *Solid State Commun.* **2010**, *150*, 1439−1444.
(32) Wang, J. G.; Ma, L.; Zhao, J. J.; Wang, G. H.; Chen, X. S.; Bruce King, R. Electronic and Magnetic Properties of Manganese and Iron-Doped Ga_nAs_n Nanocages (n = 7−12). *J. Chem. Phys.* **2008**, *129*, 044908.
(33) Ji, W. X.; Luo, C. L. Structures, Magnetic Properties, and Electronic Counting Rule of Metals-Encapsulated Cage-Like M_2Si_{18} (M = Ti-Zn) Clusters. *Int. J. Quantum Chem.* **2012**, *112*, 2525−2531.
(34) Kumar, V.; Kawazoe, Y. Hydrogenated Silicon Fullerenes: Effects of H on the Stability of Metal-Encapsulated Silicon Clusters. *Phys. Rev. Lett.* **2003**, *90*, 055502.
(35) Huang, X. M.; Xu, H. G.; Lu, S. J.; Su, Y.; King, R. B.; Zhao, J. J.; Zheng, W. J. Discovery of a Silicon-Based Ferrimagnetic Wheel Structure in $V_xSi_{12}^-$ (X = 1−3) Clusters: Photoelectron Spectroscopy and Density Functional Theory Investigation. *Nanoscale* **2014**, *6*, 14617−21.
(36) Ashcroft, N.; Mermin, N. D. *Solid State Physics*; Thomson Learning, Inc: New York, 1976.
(37) Billas, I. M.; Chatelain, A.; de Heer, W. A. Magnetism from the Atom to the Bulk in Iron, Cobalt, and Nickel Clusters. *Science* **1994**, *265*, 1682−1684.
(38) Qiang, S.; Jin, L.; Haishun, W. Density Functional Theory Study on the Structure and Magnetic Properties of Fe_2Ge_n Clusters. (in Chinese) 2014, Sciencepaper Online http://www.paper.edu.cn/html/releasepaper/2014/02/225/.
(39) Xu, H.-G.; Zhang, Z.-G.; Feng, Y.; Yuan, J.; Zhao, Y.; Zheng, W. Vanadium-Doped Small Silicon Clusters: Photoelectron Spectroscopy and Density-Functional Calculations. *Chem. Phys. Lett.* **2010**, *487*, 204−208.
(40) (a) Zhao, J. J.; Shi, R. L.; Sai, L. W.; Huang, X. M.; Su, Y. Comprehensive Genetic Algorithm for Ab Initio Global Optimisation of Clusters. *Mol. Simul.* **2016**, *42*, 809−819. (b) Yoo, S.; Zhao, J. J.; Wang, J. L.; Zeng, X. C. Endohedral silicon fullerenes Si_N (27 < N < 39). *J. Am. Chem. Soc.* **2004**, *126*, 13845−13849. (c) Yoo, S.; Zeng, X. C. Search for global-minimum geometries of medium-sized germanium clusters. II. Motif-based low-lying clusters Ge_{21}-Ge_{29}. *J. Chem. Phys.* **2006**, *124*, 184309. (d) Gao, Y.; Bulusu, S.; Zeng, X. C. Global Search of Highly Stable Gold-Covered Bimetallic Clusters $M@Au_n$ (n = 9-17). *ChemPhysChem* **2006**, *7*, 2275−2278.
(41) Zhao, J. J.; Xie, R. H. Genetic Algorithms for the Geometry Optimization of Atomic and Molecular Clusters. *J. Comput. Theor. Nanosci.* **2004**, *1*, 117−131.

DOI: 10.1021/acs.jpcc.7b00943
J. Phys. Chem. C 2017, 121, 7037−7046

(42) Sai, L. W.; Zhao, J. J.; Huang, X. M.; Wang, J. Structural Evolution and Electronic Properties of Medium-Sized Gallium Clusters from Ab Initio Genetic Algorithm Search. *J. Nanosci. Nanotechnol.* **2012**, *12*, 132−137.
(43) Sai, L. W.; Tang, L. L.; Zhao, J. J.; Wang, J.; Kumar, V. Lowest-Energy Structures and Electronic Properties of Na-Si Binary Clusters from Ab Initio Global Search. *J. Chem. Phys.* **2011**, *135*, 184305.
(44) Huang, X. M.; Lu, S.-J.; Liang, X. Q.; Su, Y.; Sai, L. W.; Zhang, Z.-G.; Zhao, J. J.; Xu, H.-G.; Zheng, W. J. Structures and Electronic Properties of $V_3Si_n^-$ (n = 3−14) Clusters: A Combined Ab Initio and Experimental Study. *J. Phys. Chem. C* **2015**, *119*, 10987−10994.
(45) Huang, X. M.; Su, Y.; Sai, L. W.; Zhao, J. J.; Kumar, V. Low-Energy Structures of Binary Pt−Sn Clusters from Global Search Using Genetic Algorithm and Density Functional Theory. *J. Cluster Sci.* **2015**, *26*, 389−409.
(46) Hong, L.; Wang, H. L.; Cheng, J. X.; Huang, X. M.; Sai, L. W.; Zhao, J. J. Atomic Structures and Electronic Properties of Small Au−Ag Binary Clusters: Effects of Size and Composition. *Comput. Theor. Chem.* **2012**, *993*, 36−44.
(47) Wu, X.; Lu, S.-J.; Liang, X. Q.; Huang, X. M.; Qin, Y.; Chen, M. D.; Zhao, J. J.; Xu, H.-G.; King, R. B.; Zheng, W. J. Structures and electronic properties of $B_3Si_n^-$ (n = 4−10) clusters: A combined ab initio and experimental study. *J. Chem. Phys.* **2017**, *146*, 044306.
(48) Perdew, J. P.; Burke, K.; Ernzerhof, M. Generalized Gradient Approximation Made Simple. *Phys. Rev. Lett.* **1996**, *77*, 3865.
(49) Delley, B. An All-Electron Numerical Method for Solving the Local Density Functional for Polyatomic Molecules. *J. Chem. Phys.* **1990**, *92*, 508−517.
(50) Delley, B. From Molecules to Solids with the $Dmol^3$ Approach. *J. Chem. Phys.* **2000**, *113*, 7756−7764.
(51) Oda, T.; Pasquarello, A.; Car, R. Fully Unconstrained Approach to Noncollinear Magnetism: Application to Small Fe Clusters. *Phys. Rev. Lett.* **1998**, *80*, 3622.
(52) Diéguez, O.; Alemany, M. M. G.; Rey, C.; Ordejón, P.; Gallego, L. J. Density-Functional Calculations of the Structures, Binding Energies, and Magnetic Moments of Fe Clusters with 2 to 17 Atoms. *Phys. Rev. B: Condens. Matter Mater. Phys.* **2001**, *63*, 205407.
(53) Cox, D.; Trevor, D.; Whetten, R.; Rohlfing, E.; Kaldor, A. Magnetic Behavior of Free-Iron and Iron Oxide Clusters. *Phys. Rev. B: Condens. Matter Mater. Phys.* **1985**, *32*, 7290.
(54) Purdum, H.; Montano, P. A.; Shenoy, G. K.; Morrison, T. Extended-X-Ray-Absorption-Fine-Structure Study of Small Fe Molecules Isolated in Solid Neon. *Phys. Rev. B: Condens. Matter Mater. Phys.* **1982**, *25*, 4412−4417.
(55) Froben, F. W.; Schulze, W. Matrix-Isolation Spectroscopy of Germanium Molecules. *Surf. Sci.* **1985**, *156*, 765−769.
(56) Leopold, D. G.; Lineberger, W. C. A Study of the Low-Lying Electronic States of Fe_2 and Co_2 by Negative Ion Photoelectron Spectroscopy. *J. Chem. Phys.* **1986**, *85*, 51−55.
(57) Arnold, C. C.; Xu, C.; Burton, G. R.; Neumark, D. M. Study of the Low-Lying States of Ge_2 and Ge^-_2 Using Negative Ion Zero Electron Kinetic Energy Spectroscopy. *J. Chem. Phys.* **1995**, *102*, 6982−6989.
(58) Lin, S.-S.; Kant, A. Dissociation Energy of Fe_2. *J. Phys. Chem.* **1969**, *73*, 2450−2451.
(59) Hunter, J. M.; Fye, J. L.; Jarrold, M. F.; Bower, J. E. Structural Transitions in Size-Selected Germanium Cluster Ions. *Phys. Rev. Lett.* **1994**, *73*, 2063−2066.
(60) Donohue, J. *Structures of the Elements*; Wiley: New York, 1974; Vol. *7*.
(61) Kittel, C. *Introduction to Solid State Physics*, 6th ed.; translated by Uno, Y., Tsuya, N., Morita, A., Yamashita, J.; Maruzen: Tokyo, 1986; pp 124−129.
(62) Frisch, M. J.; Trucks, G. W.; Schlegel, H. B.; Scuseria, G. E.; Robb, M. A.; Cheeseman, J. R.; Scalmani, G.; Barone, V.; Mennucci, B.; Petersson, G. A., et al. *Gaussian 09*, revision D.01; Gaussian, Inc.: Wallingford, CT, 2009.
(63) Jing, Q.; Tian, F.-Y.; Wang, Y.-X. No Quenching of Magnetic Moment for the Ge_nCo (n = 1−13) Clusters: First-Principles Calculations. *J. Chem. Phys.* **2008**, *128*, 124319−124319.

DOI: 10.1021/acs.jpcc.7b00943
J. Phys. Chem. C 2017, 121, 7037−7046